New Measurements of the European Muon Collaboration Effect in Very Light Nuclei

J. Seely,[1] A. Daniel,[2] D. Gaskell,[3] J. Arrington,[4,*] N. Fomin,[5] P. Solvignon,[4] R. Asaturyan,[6,†] F. Benmokhtar,[7] W. Boeglin,[8]
B. Boillat,[9] P. Bosted,[3] A. Bruell,[3] M. H. S. Bukhari,[2] M. E. Christy,[10] B. Clasie,[1] S. Connell,[5,‡] M. M. Dalton,[5] D. Day,[5]
J. Dunne,[11] D. Dutta,[11,12] L. El Fassi,[4] R. Ent,[3] H. Fenker,[3] B. W. Filippone,[13] H. Gao,[1,12] C. Hill,[5] R. J. Holt,[4] T. Horn,[7,3]
E. Hungerford,[2] M. K. Jones,[3] J. Jourdan,[9] N. Kalantarians,[2] C. E. Keppel,[10] D. Kiselev,[9] M. Kotulla,[9] C. Lee,[14]
A. F. Lung,[3] S. Malace,[10] D. G. Meekins,[3] T. Mertens,[9] H. Mkrtchyan,[6] T. Navasardyan,[6] G. Niculescu,[15] I. Niculescu,[15]
H. Nomura,[16] Y. Okayasu,[2,16] A. K. Opper,[17] C. Perdrisat,[18] D. H. Potterveld,[4] V. Punjabi,[19] X. Qian,[12] P. E. Reimer,[4]
J. Roche,[3] V. M. Rodriguez,[2] O. Rondon,[5] E. Schulte,[4] E. Segbefia,[10] K. Slifer,[5] G. R. Smith,[3] V. Tadevosyan,[6] S. Tajima,[5]
L. Tang,[10] G. Testa,[9] R. Trojer,[9] V. Tvaskis,[10] W. F. Vulcan,[3] F. R. Wesselmann,[5] S. A. Wood,[3] J. Wright,[5]
L. Yuan,[10] and X. Zheng[4]

[1]*Laboratory for Nuclear Science, Massachusetts Institute of Technology, Cambridge, Massachusetts, USA*
[2]*University of Houston, Houston, Texas, USA*
[3]*Thomas Jefferson National Laboratory, Newport News, Virginia, USA*
[4]*Physics Division, Argonne National Laboratory, Argonne, Illinois, USA*
[5]*University of Virginia, Charlottesville, Virginia, USA*
[6]*Yerevan Physics Institute, Yerevan, Armenia*
[7]*University of Maryland, College Park, Maryland, USA*
[8]*Florida International University, Miami, Florida, USA*
[9]*Basel University, Basel, Switzerland*
[10]*Hampton University, Hampton, Virginia, USA*
[11]*Mississippi State University, Jackson, Mississippi, USA*
[12]*Triangle Universities Nuclear Laboratory, Duke University, Durham, North Carolina, USA*
[13]*Kellogg Radiation Laboratory, California Institute of Technology, Pasadena, California, USA*
[14]*University of the Witwatersrand, Johannesburg, South Africa*
[15]*James Madison University, Harrisonburg, Virginia, USA*
[16]*Tohoku University, Sendai, Japan*
[17]*Ohio University, Athens, Ohio, USA*
[18]*College of William and Mary, Williamsburg, Virginia, USA*
[19]*Norfolk State University, Norfolk, Virginia, USA*

New Jefferson Lab data are presented on the nuclear dependence of the inclusive cross section from ^{2}H, ^{3}He, ^{4}He, ^{9}Be and ^{12}C for $0.3 < x < 0.9$, $Q^2 \approx 3$–6 GeV^2. These data represent the first measurement of the EMC effect for ^{3}He at large x and a significant improvement for ^{4}He. The data do not support previous A-dependent or density-dependent fits to the EMC effect and suggest that the nuclear dependence of the quark distributions may depend on the *local* nuclear environment.

High energy lepton scattering provides a clean method of probing the quark momentum distributions in nucleons and nuclei. The early expectation was that probes at the GeV energy scale would be insensitive to nuclear binding effects, which are typically on the order of several MeV. The effects were expected to be small except at large Björken-x, corresponding to very high momentum quarks. In this region, the rapid falloff of the parton distributions approaching the kinematical limit of $x \rightarrow 1$ makes the distributions very sensitive to the smearing effect of the nucleon's motion.

In 1983 the European Muon Collaboration (EMC) discovered that the per-nucleon deep inelastic structure function, $F_2(x)$, in iron was significantly different than that for deuterium [1]. They showed a clear suppression of high momentum quarks for $0.3 < x < 0.8$, confirmed for several

nuclei in more extensive measurements at SLAC [2]. This phenomenon, dubbed the "EMC effect," has become the subject of a determined theoretical effort aimed at understanding the underlying physics. While progress has been made in explaining the principal features of the effect, no single model has been able to explain the effect over all x and A [3,4]. Much of the effort has focused on heavy nuclei, and many models are evaluated for infinite nuclear matter and scaled to the density of finite nuclei, neglecting possible surface effects or the impact of detailed nuclear structure.

There has been less focus on few-body nuclei, which provide the opportunity to test models in cases where the details of the nuclear structure are well understood. These data are also necessary to get a complete picture of the evolution of nuclei from deuterium to infinite nuclear

matter. Precise measurements in few-body nuclei allow for stringent tests of calculations of the effects of Fermi motion and nuclear binding, which is the dominant effect at large x. In addition, these data allow us to test simple scaling models of the EMC effect. A global analysis of the SLAC data [2] found that the data could be equally well described by fits that assumed the EMC effect to be proportional to the average nuclear density, ρ, or by fits that assumed it scaled with the nuclear mass, i.e., an EMC effect proportional to $\ln(A)$. These simple fits for the nuclear dependence did equally well for heavy nuclei ($A \gtrsim 12$), where the density varies slowly with A. For very light nuclei, these simple models predict different behavior, but the limited data on light nuclei were not sufficient to differentiate between these predictions.

To address these issues, Jefferson Lab (JLab) experiment E03-103 was proposed to make high precision measurements of the EMC effect at large x in both heavy and few-body nuclei. The experiment ran in Hall C during the fall of 2004. The measurement used a 5.767 GeV, 80 μA unpolarized electron beam, with scattered electrons detected in the High Momentum Spectrometer (HMS). The primary measurements were taken at a scattering angle of 40°, with additional data taken at different angles and/or 5 GeV beam energy to examine the Q^2 dependence. Data were collected on four cryotargets—^{1}H, ^{2}H, ^{3}He, and ^{4}He, and solid Beryllium, Carbon, Copper, and Gold targets arranged together on a common target ladder. The target ladder held only two cryotargets at a time, so there were two separate running periods to collect data on all four cryogenic targets. Data were taken on solid targets during both periods for systematic checks on the relative normalization during the two run periods. In this Letter, we focus on the light nuclei, $A \leq 12$, for which fewer data exist and which require smaller corrections due to backgrounds and Coulomb distortion.

The HMS subtends a solid angle of 7 msr and the momentum bite was restricted to the central part of the acceptance ($\pm 9\%$). The detector package consisted of two sets of wire chambers for tracking, four planes of hodoscopes for triggering, and a gas Čerenkov and lead-glass calorimeter for online and offline particle identification [5]. The cross sections were corrected for electronic and computer dead times, detector efficiencies, and radiative effects (which closely followed the approach of Ref. [6]). Data were taken at several beam currents on carbon to look for rate-dependent corrections, and on all four cryotargets to measure current-dependent target density effects due to heating at high current.

The dominant sources of background were pion production, electrons scattering from the aluminum cryocell wall and electrons from pair-production in the target. After applying calorimeter and Čerenkov cuts, the pion contamination was negligible for the kinematics shown here. The electron background (8%–19%) from the cell wall was subtracted using measurements on a ''dummy'' target, consisting of two aluminum targets at the positions of the cryocell walls, with radiative corrections calculated separately for the real cryocells and the dummy target. The background from pair production was measured by reversing the HMS polarity to detect positrons, yielding a direct measure of the charge-symmetric background, strongly dominated by pair production. This background was typically 5%–10%, but was as much as 30% of the total yield at the lowest x and largest Q^2 values.

There are several sources of systematic uncertainty which we separate into point-to-point and normalization uncertainties. Normalization uncertainties are those that modify the overall scale, but not the x or Q^2 dependence of the target cross section ratios, e.g., target thicknesses. Point-to-point uncertainties can vary with x or Q^2, and are treated in the same way as statistical uncertainties.

The cryogenic target thicknesses were determined from the dimensions of the cryocell and the density of the cryogen, as computed from measurements of its pressure and temperature. The total normalization uncertainty in the cross section ratios was between 1.6% and 1.9%, mainly due to the 1%–1.5% uncertainty in the target thicknesses. Uncertainty in the target boiling correction contributes $\sim 0.4\%$, radiative corrections [6] contribute 0.1%–0.75%, depending on the kinematics and target thickness, and the acceptance contributes 0.5% (0.2%) to the solid target (cryotarget) ratios. The dominant sources of point-to-point uncertainties come from charge measurement drifts (0.3%), corrections due to drift of beam position on target (0.45%), radiative corrections (0.5%), dead time determination (0.3%), detector efficiencies (0.3%), and acceptance (0.3%). Charge-symmetric background subtraction contributes 0.1%–0.6% to the uncertainty, and is largest for the Be and C targets. The uncertainties in the kinematics contribute up to 0.6% to the uncertainties in the ratios, with larger effects at large x values where the cross section is changing most rapidly. We apply Coulomb distortion corrections following the effective momentum approximation of Aste [7]. The corrections are $\lesssim 1\%$ for ^{12}C, and much smaller for the helium data.

The results are shown as ratios of the cross section per nucleon, rather than the F_2 structure functions. These ratios are identical if the ratio of longitudinal to transverse cross sections, $R = \sigma_L / \sigma_T$, is independent of A. If $R_A \neq R_D$, then there will be a correction involved in going from cross section ratios to the F_2 ratios [3].

In the Björken limit, the structure function exhibits scaling, i.e., becomes independent of Q^2 except for the weak Q^2 dependence from QCD evolution of the parton distributions. This scaling has been observed in the deep-inelastic scattering region, which for e-p scattering is typically taken to be $Q^2 > 1$ GeV^2 and $W^2 > 4$ GeV^2, where W is the invariant mass of the unmeasured system. In nuclei, it has been observed that results are nearly

independent of Q^2 to lower values of W^2 for $Q^2 \gtrsim 3$ GeV^2 [8]. A precise measurement of the target ratios in the resonance region [9] for $Q^2 = 3$–4 GeV^2 showed that the nuclear dependence is identical to the high Q^2 measurements up to $x \approx 0.8$, even though the deep-inelastic scattering region is limited to $x < 0.5$ for these Q^2 values.

Because these data are at somewhat lower Q^2 than previous high-x results, typically $Q^2 = 5$ or 10 GeV^2 for SLAC E139 [2], extensive measurements were made to verify that our result is independent of Q^2. The structure functions were extracted at several Q^2 values and found to be consistent with scaling violations expected from QCD down to $Q^2 \approx 3$ GeV^2 for $W^2 \geq 1.5$ GeV^2, while the structure functions ratios show no Q^2 dependence. Figure 1 shows the carbon to deuteron ratio for the five highest Q^2 settings (the lowest and middle Q^2 values were measured with a 5 GeV beam energy). There is no systematic Q^2 dependence in the EMC ratios, even at the largest x values, consistent with the observation of previous measurements [3].

For all further results, we show the ratios obtained from the 40° data (filled squares in Fig. 1). While there are data at 50° (open circles) for all nuclei, the statistical precision is much worse, and there are much larger corrections for charge-symmetric background and Coulomb distortion (for heavier nuclei).

The EMC ratios for ^{12}C, ^{9}Be, and ^{4}He are shown in Fig. 2 along with results from previous SLAC extractions. The ^{4}He and ^{12}C results are in good agreement with the SLAC results, with much better precision for ^{4}He in the new results. While the agreement for ^{9}Be does not appear to be as good, the two data sets are in excellent agreement if we use the same isoscalar correction as E139 (see below) and take into account the normalization uncertainties in the two data sets. In all cases, the new data extend to higher x, although at lower W^2 values than the SLAC ratios. The

EMC ratio for ^{4}He is comparable to ^{12}C, suggesting that the modification is dependent on the average nuclear density, which is similar for ^{4}He and ^{12}C, rather than a function of nuclear mass.

Figure 3 shows the EMC ratio for ^{3}He, with the low-x data from HERMES. Note that the HERMES ^{3}He data have been renormalized by a factor of 1.009 based on comparisons of their ^{14}N EMC effect and the New Muon Collaboration ^{12}C result [10]. We show both the measured cross section ratio (squares) and the "isoscalar" ratio (circles), where the ^{3}He result is corrected for the proton excess. Previous high-x EMC measurements used a correction based on an extraction of the F_{2n}/F_{2p} ratio for free nucleons from high Q^2 measurements of F_{2d}/F_{2p}. We use global fits [11,12] to the free proton and neutron cross sections evaluated at the kinematics of our measurement and then broadened using the convolution procedure of

FIG. 2 (color online).   EMC ratios for ^{12}C, ^{9}Be, and ^{4}He [17], compared to SLAC [2]. The ^{9}Be results include a correction for the neutron excess (see text). Closed (open) circles denote W^2 above (below) 2 GeV^2. The solid curve is the A-dependent fit to the SLAC data, while the dashed curve is the fit to ^{12}C. Normalization uncertainties are shown in parentheses for both measurements.
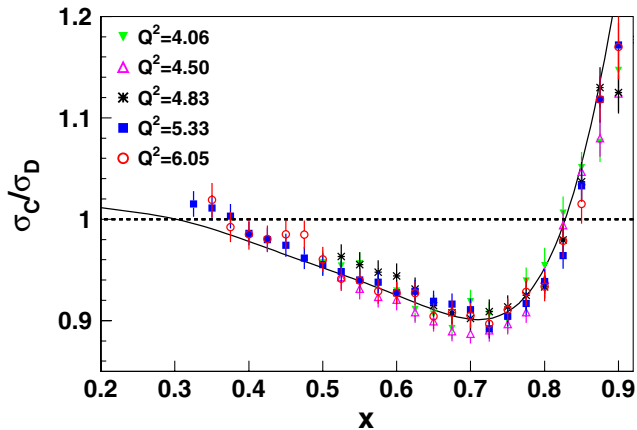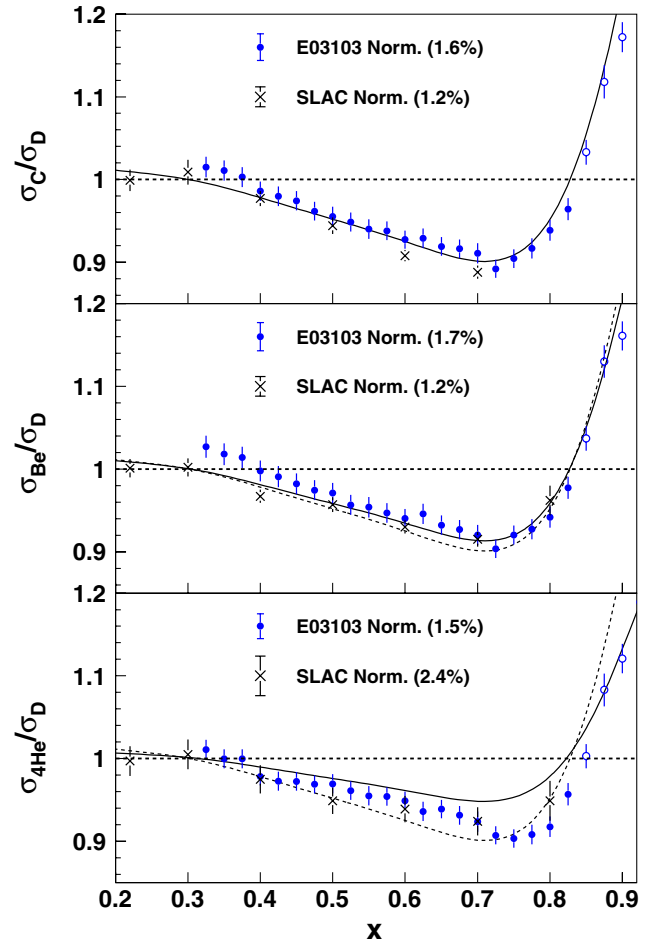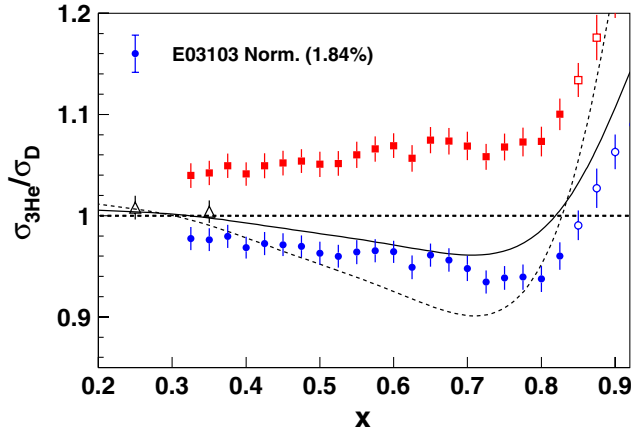

FIG. 1 (color online).   Carbon EMC ratios [17] for the five highest Q^2 settings (Q^2 quoted at $x = 0.75$). Uncertainties are the combined statistical and point-to-point systematic. The solid curve is the SLAC fit [2] to the Carbon EMC ratio.

FIG. 3 (color online). EMC ratio for ^{3}He [17]. The upper squares are the raw ^{3}He/^{2}H ratios, while the bottom circles show the isoscalar EMC ratio (see text). The triangles are the HERMES results [10] which use a different isoscalar correction. The solid (dashed) curves are the SLAC A-dependent fits to carbon and ^{3}He.

Ref. [13] to yield the neutron-to-proton cross section ratio in nuclei. Using the "smeared" proton and neutron cross section ratios more accurately reflects the correction that should be applied to the nuclear ratios, and in the end, yields a significantly smaller correction at large x, where the uncertainty in the neutron structure function is largest.

While applying the isoscalar correction to the ^{3}He data using the smeared F_{2n}/F_{2p} ratio yields a more reliable result, there is still some model dependence to this correction due to the uncertainty in our knowledge of the neutron structure function. Ref. [13] demonstrated that much of the inconsistency between different extractions of the neutron structure function comes from comparing fixed-Q^2 calculation to data with varying Q^2 values, rather than from the underlying assumptions of nuclear effects in the deuteron. Nuclear effects beyond what is included in Ref. [13], such as the off-shell contribution $\delta^{(\text{off})}$ of Ref. [14], yield a 1%–2% decrease to the proton's contribution to the deuteron thus increasing the extracted F_{2n}/F_{2p} ratio by 0.01–0.02. This yields a slightly reduced correction for ^{3}He which would raise the isoscalar EMC ratio for ^{3}He by 0.3%–0.6% at our kinematics.

The observed nuclear effects are clearly smaller for ^{3}He than for ^{4}He and ^{12}C. This is again consistent with models where the EMC effect scales with the average density, as the average density for ^{3}He is roughly half that of the ^{12}C. However, the results of ^{9}Be are not consistent with the simple density-dependent fits. The observed EMC effect in ^{3}He is essentially identical to what is seen in ^{12}C, even though the density of ^{9}Be is much lower. This suggests that both the simple mass- or density-scaling models break down for light nuclei.

One can examine the nuclear dependence based on the size of the EMC ratio at a fixed x value, but the normal-

ization uncertainties become a significant limiting factor. If we assume that the shape of the EMC effect is universal, and only the magnitude varies with target nucleus, we can compare light nuclei by taking the x dependence of the ratio in the linear region, $0.35 < x < 0.7$, using the slope as a measure of the relative size of the EMC effect that is largely unaffected by the normalization. The slopes are shown for light nuclei in Fig. 4 as a function of average nuclear density. The average density is calculated from the *ab initio* Greens Function Monte Carlo calculation of the spatial distributions [15]. Because we expect that it is the presence of the other $(A − 1)$ nucleons that yields the modification to the nuclear structure function, we choose to scale down this density by a factor of $(A − 1)/A$, to remove the struck nucleon's contribution to the average density. The EMC effect for ^{3}He is roughly one third of the effect in ^{4}He, in contrast to the A-dependent fit to the SLAC data [2], while the large EMC effect in ^{9}Be contradicts a simple density-dependent effect.

One explanation for the anomalous behavior of ^{9}Be is that it can be described as a pair of tightly bound alpha particles plus one additional neutron [16]. While most of the nucleons are in a dense environment, similar to ^{4}He, the *average* density is much lower, as the alphas (and additional neutron) "orbit" in a larger volume. This suggests that it is the *local* density that drives the modification. The strong clustering of nucleons in ^{9}Be leads to a special case where the average density does not reflect the local environment of the bulk of the protons and neutrons.

Another possibility is that the x dependence of the EMC effect is different enough in these light nuclei that we cannot use the falloff with x as an exact measure of the relative size of the EMC effect. This too suggests that the EMC effect is sensitive to the details of the nuclear structure, which would require further theoretical examination. At the moment, there are almost no calculations for light nuclei that include detailed nuclear structure.
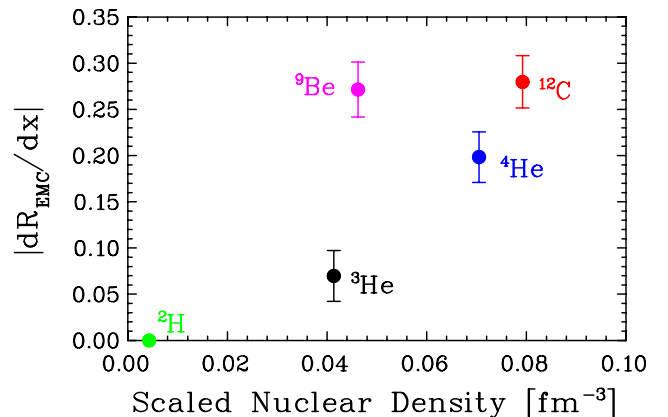

FIG. 4 (color online). The circles show the slope of the isoscalar EMC ratio for $0.35 < x < 0.7$ as a function of nuclear density. Error bars include statistical and systematic uncertainties.

In conclusion, we have measured the nuclear dependence of the structure functions for a series of light nuclei. This data set provides significantly improved data on ^{4}He and the first valence-region measurement on ^{3}He, as well as extending the measurements to higher x for other light nuclei. This will allow for more detailed comparison with calculations that include binding and Fermi motion, providing a more reliable baseline at low x, where these effects are still important, but may not fully explain the observed nuclear dependence.

These data also provide model independent information on the scaling of the nuclear effects. Under the assumption that the shape of the EMC effect is the same for all nuclei, the large difference between ^{3}He and ^{4}He rules out previous A-dependent fits, while the EMC effect in ^{9}Be is inconsistent with models where the effect scales with average density. The results are consistent with the idea that the effect scales with the *local* environment of the nucleons, or require that the x dependence of the effect changes in very light nuclei.

*Corresponding author: johna@anl.gov
†Deceased
‡Present address: University of Johannesburg, Johannesburg, South Africa.

[1] J. Aubert *et al.*, Phys. Lett. B **123**, 275 (1983).
[2] J. Gomez *et al.*, Phys. Rev. D **49**, 4348 (1994).
[3] D. F. Geesaman, K. Saito, and A. W. Thomas, Annu. Rev. Nucl. Part. Sci. **45**, 337 (1995).
[4] P. R. Norton, Rep. Prog. Phys. **66**, 1253 (2003).
[5] D. Dutta *et al.*, Phys. Rev. C **68**, 064603 (2003).
[6] S. Dasu *et al.*, Phys. Rev. D **49**, 5641 (1994).
[7] A. Aste, C. von Arx, and D. Trautmann, Eur. Phys. J. A **26**, 167 (2005).
[8] J. Arrington *et al.*, Phys. Rev. C **64**, 014602 (2001).
[9] J. Arrington, R. Ent, C. E. Keppel, J. Mammei, and I. Niculescu, Phys. Rev. C **73**, 035205 (2006).
[10] K. Ackerstaff *et al.* (HERMES), Phys. Lett. B **475**, 386 (2000); **567**, 339(E) (2003).
[11] M. E. Christy and P. E. Bosted arXiv:0712.3731.
[12] P. E. Bosted and M. E. Christy, Phys. Rev. C **77**, 065206 (2008).
[13] J. Arrington, F. Coester, R. J. Holt, and T. S. H. Lee, J. Phys. G **36**, 025005 (2009).
[14] W. Melnitchouk, A. W. Schreiber, and A. W. Thomas, Phys. Lett. B **335**, 11 (1994).
[15] S. C. Pieper and R. B. Wiringa, Annu. Rev. Nucl. Part. Sci. **51**, 53 (2001).
[16] K. Arai, Y. Ogawa, Y. Suzuki, and K. Varga, Phys. Rev. C **54**, 132 (1996).
[17] See EPAPS Document No. E-PRLTAO-103-015948 for data tables and figures. They are also available for download at http://hallcweb.jlab.org/experiments/E03103. For more information on EPAPS, see http://www.aip.org/pubservs/epaps.html.